================================ **METALS** ================================

Structure and Magnetic Properties of Nanowires of Iron Group Metals Produced by Matrix Synthesis

D. L. Zagorskiy[a], *, K. V. Frolov[a], S. A. Bedin[a, b], I. V. Perunov[a], M. A. Chuev[c],
A. A. Lomov[c], and I. M. Doludenko[a, d]

[a] *Shubnikov Institute of Crystallography, Federal Research Center "Crystallography and Photonics,"*
Russian Academy of Sciences, Moscow, Russia
[b] *Moscow Pedagogical State University, Moscow, Russia*
[c] *Institute of Physics and Technology of RAS, Russian Academy of Sciences, Moscow, Russia*
[d] *National Research Institute, Moscow, Russia*
*e-mail: dzagorskiy@gmail.com
Received May 14, 2018

Abstract—Samples of arrays of nanowires are produced from iron, iron–cobalt and iron–nickel alloys via matrix synthesis based on polymer track membranes with pore diameters ranging from 30 to 300 nm. The influence of stress and pore diameter on the galvanic process and structure of nanowires is studied. The arrays of nanowires are examined by microscopy and X-ray diffraction. The magnetic properties are inspected via magnetometry and Mössbauer spectroscopy. The angular dependences of hysteresis loop shape are obtained and comprehensively discussed. As shown, decreasing the growth stress and/or increasing the pore diameter make the Mössbauer spectra of nanowires similar to those of bulk materials. Furthermore, the higher the growth stress is, the larger is the coercive force of nanowires. For the studied species of nanomaterials, the ability to control the magnetic properties during the synthesis is shown, as well.

1. INTRODUCTION

A so-called matrix (template) method is of particular interest among other routes of nanomaterial synthesis, whereby pores in a preprepared matrix (template) are filled with a needed substance. This allows the formation of molds (replicas) of pores, whose geometry is determined by that of pores in the matrix. Ensembles (arrays) of a large amount of elongated filaments (1D structures)—nanowires (NWs), or nanocolumns—are thereby produced. It is worth mentioning that template synthesis underlies two different—top-down and bottom-up—approaches of nanostructure formation [1]. It may involve various types of matrices, such as porous aluminum oxide, track membranes, and porous zeolites. Pores can be loaded with different substances, i.e., polymers, water-soluble crystals, semiconductors and metals, through chemical or electrochemical methods. In this work, matrices were the polymer membranes that are suitable for producing the arrays of identical NWs and for tuning their arrangement density on the surface, diameter, and geometry (if needed) in the wide ranges. Pores of these matrices were filled with nanowires of diverse metals via the electrochemical (galvanic) approach.

The idea to obtain a mold was pioneered in [2] where the authors conducted the electrochemical deposition of tin in the pores of mica. Furthermore, a successful deposition of cobalt and nickel in the matrix of porous aluminum oxide was described in [3], where the use of these structures in magnetic storage devices was proposed, as well. In the subsequent works, the electrodeposition of metals was implemented in track pores of polymer matrices [4–6]. A thorough analysis of matrix synthesis methods was expounded in the most cited review by Martin [7]. The follow-up works were dedicated to practice methods for production of replicas of pore channels and synthesis of nanowires (NWs) using various metals.

Nowadays, there are some reviews that aim the electrochemical synthesis of metal nanostuctures [8–10]. The main growth matrices are track membranes (TM) [7] and porous aluminum oxide [11].

Matrices of porous aluminum oxide are the main competitors to TMs and exhibit apparent advantages. However, the benefits of TMs, such as low cost, flexibility, small parameter variation, the ability to explore independently the geometric parameters within the wide ranges, and others, allow their use for many applications. Note that "industrial" TMs are not always suitable for template synthesis, because their basic parameters are high density of pores and their different inclination make them optimal for filtration

tasks. The template synthesis tends to smaller densities of pores and their parallel arrangement. These parameters are achievable within the matrix formation, when a polymer film is exposed to irradiation. Thus, purposely prepared matrices are explored in template synthesis.

The range of potential applications of NW arrays is very wide due to their unique properties, such as developed surface area. In this case, one feasible application is the creation of surfaces for catalysis and heat sink [12]. Another property is the small curvature radius of a multiplicity of identical tips that allows for the formation of electron emitters (cold cathodes) [13] or ion emission surfaces [14]. The synthesis of nanostructures with specific magnetic properties, e.g., magnetic sensors, giant magnetic resistance devices, and high density magnetic recording surfaces, is also promising. Nanowires for these purposes are produced from metals typically attributed to the iron group, such as pure iron, cobalt, nickel, as well as their compounds.

One pioneering work on the synthesis of iron NWs was performed in [15]. The iron electrodeposition peculiarities, the structure of obtained NWs and their magnetic properties were reported in [16]. The deposition of cobalt and nickel was first described in [3]. The electrodeposition features of thee metals in pores of track membranes were within the scope of various studies, e.g., [17, 18]. The subsequent step was the production of NWs using two (or more) metals, i.e., multicomponent NWs. It is worth noting that exploring electrolytes based on two or several salts and tuning the deposition potential in the galvanic method allow the changes of synthesis conditions and the obtainment of various types of NWs. For instance (in the simplest case of two-component electrolytes), at a constant potential exceeding the deposition potential of both metals, the latter are jointly deposited, forming a so-called "alloy." On the other hand, the periodical variation of the growth voltage enables the alternating layer-by-layer deposition of a pure metal layer and a mixed composition layer with a tunable component ratio. This makes it possible to obtain the so-called "layered" NW structures that seem interesting and promising for practical applications. However, the consideration of these wafer structures is beyond the scope of this work.

The synthesis of NW arrays of iron−cobalt alloys (55% Fe) was described in [19], where NWs with diameters of 20 to 200 nm were grown in pores of the aluminum oxide matrix. Their structure and magnetic properties were elucidated as well. The saturation magnetization was measured to be 22−24 kGs, almost attaining the parameter for the bulk material of the same composition. The growth peculiarities in pores of track membranes, the structure, and some magnetic properties of Fe−Co NWs were reported in [20]. The synthesis of nanowires of the iron−nickel alloy was described by numerous groups. So, the production of

porous aluminum oxide matrices and the synthesis of NWs in the pulsed mode were detailed in [21]. In [22], iron−nickel NWs were also grown in the pulsed mode of deposition, which was compared to the growth in alternating current. The influence of the composition on the magnetic properties and structure of NWs was studied as well. As shown, the coercive force enriched its maximum value at the nickel content of 3%. The nickel content above 30% led to the formation of the phase with an fcc lattice. In [23], Fe−Ni NWs were grown at using the alternating current and were shown to exhibit the high magnetic anisotropy. For a magnetic field oriented along the NW axis, the coercive force and the remaint magnetization achieve their maxima. In most cases, the growth was conducted in matrices of porous aluminum oxide.

In order to study the magnetic properties of iron-containing NWs in combination with conventional magnetometry, it seems expedient to explore a sensitive tool, such as Mössbauer spectroscopy. In recent years, a number of such works is very small [16, 20, 24−26], mainly for NWs obtained in the aluminum oxide matrix under substantially different conditions.

It can therefore be concluded that, despite the prospects in using NW arrays of iron group metals and a large amount of items published in this field of research, some questions remain still unclear. In many foreign works, the synthesis is mainly conducted with the use of porous aluminum oxide, while the unique abilities to explore track membranes are almost unknown. The influence of synthesis conditions on structure and properties of produced NW arrays is poorly studied as well. In this connection, this work is aimed at obtaining NW arrays from iron, iron−cobalt and iron−nickel alloys via the polymer membrane synthesis and at investigating their structure.

2. MATERIALS AND METHODS

2.1. Matrices

The template synthesis was implemented on "industrial" track membranes (TMs) fabricated at the Laboratory of Nuclear Reactions (Joint Institute of Nuclear Research, Dubna) made of the PETP film with a thickness of about 10 μm; the pore diameter reported by the producer ranged from 30 to 200 nm, and the pore density was on the order of 10^8 pores/cm^2. The matrices of the low-density irradiation film were also used to obtain the matrices with a pore density of $10^6 - 10^7$ per cm^2).

The conductive layer on the TM surface was created as follows: one side of the membrane was covered with a thin copper layer via the thermal sputtering in vacuum on a VUP-4 setup. This layer was optionally increased by successive galvanic deposition of a copper layer with a thickness of several microns.

2.2. Electric Deposition

For the electric deposition, electrolytes based on sulfates of the corresponding metals were used. Most compounds described below and not reported here (tests reveal their low efficiency) were taken from the literature (e.g., from [27]). The utilized compositions and synthesis modes are outlined below.

The iron nanowire arrays were produced from $FeSO_4 \cdot 7H_2O$ (200 g/L) and $AlCl_3 \cdot 6H_2O$ (50 g/L) electrolytes. The galvanic process was conducted at room temperature at pH = 2.5 in the electric deposition mode at a fixed potential range of -600 to -1050 mV. The first data gathered in a study with this electrolyte are presented in [16].

The peculiar features of iron deposition are as follows. Since Fe^{2+} ions oxidize to Fe^{3+} by the air oxygen, iron is thus a quite complex metal for the galvanic deposition because of the instability of the electrolyte. This reaction is undesirable, due to the fact that Fe^{3+} ions are prone to strong hydrolysis that causes the inclusion of oxygen in the form of iron hydroxides in the metal precipitation. Hydrolysis is particularly active in a near-cathode area where releasing hydrogen leads to alkalinization. The negative impact of alkalinization can be reduced by increasing the acidity of solution, using buffer additives (e.g., salts of aluminum). Some reducing agents (antioxidants) allow the oxidation of Fe^{2+} to Fe^{3+} to be avoided.

The iron−cobalt nanowire arrays were produced from the chloride sulfate electrolyte with a Fe^{2+} : Co^{2+} component ratio of 0.54 : 0.18 mol/L at room temperature. The electrolyte composition was as follows: $FeSO_4 \cdot 7H_2O$ (150 g/L), $CoCl_2 \cdot 6H_2O$ (42.7 g/L), and $AlCl_3 \cdot 6H_2O$ (40g/L). The deposition was conducted at pH of 1.2−1.9 in the potentiostatic mode at potentials ranging from -700 to -900 mV. The earlier results of the work with this electrolyte are available in [20].

The electric deposition of iron−nickel alloy was implemented from the electrolyte composed of $NiSO_4 \cdot 7H_2O$ (16 g/L), $NiCl_2 \cdot 6H_2O$ (40 g/L), $FeSO_4 \cdot 7H_2O$ (1 g/L), H_3BO_3 (25 g/L); at pH = 2.4 at room temperature in the potentiostatic mode at potentials on a cell from 1000 to 1500 mV. The iron salt ($FeSO_4 \cdot 7H_2O$) content varied from 1 to 16 g/L, which enabled the production of NWs with different component ratios.

The described electrolytes were chosen among the standard compositions reported in the literature. They serve upon the deposition of metals on a flat surface as well as in the pores of track membranes. The goal of the present work was also to select alloyings in electrolytes and the electric deposition modes.

A purposely made cell with a two-electrode connection scheme was used. The process was implemented in the potentiostatic mode, with measuring the so-called potentiostatic curves, or current plotted versus time.

2.3. Microscopy

The preliminary inspection of the surface was conducted on an optical microscope in order to select samples and to choose areas to be probed. The electron microscopy studies were based on SEM and TEM methods. The topography of samples was mainly examined on a QUANTA 200 3D scanning electron microscope equipped with an EDAX-Genesis microanalysis console (the accelerating voltage was up to 20 kV and the magnification was 2000−6000) and on a FEI Tecnai Osiris transmission electron microscope (with the accelerating voltage to 200 kV) with electron diffraction and energy-dispersion analysis (EDA) consoles. The element analysis and chemical element distribution maps were obtained on a SuperX EDS setup including four silicon detectors, whose construction allows the acquisition of large area chemical element distribution maps for several minutes. The processing and analysis of images and electronograms recorded in the electron microscope were performed using Digital Micrograph, Esprit, TIA, and JEMS software.

2.4. X-ray Diffraction Analysis

Samples were measured via different ways:

—on an X'PERT PRO (PANalytical, Netherlands) diffractometer in the Bragg−Brentano geometry using the CuK_α radiation ($\lambda = 1.5418$ Å, the Ni filter);

—on a synchrotron radiation source (Kurchatov Center of Synchrotron Radiation) at the X-ray station using the radiation wavelength $\lambda = 0.832$ Å.

In both cases, data were recorded and processed via the conventional methods.

For some samples, the spectra were shifted because of surface irregularities (a thin film with nanowires) caused by the deformation of the film itself upon its deposition, which could not be prevented while the film was fixed on a holder. In this case, the calibration over the copper lines (from the substrate) was used, which were intensive for all samples.

2.5. Magnetic Measurements of Samples

Magnetization of nanowires as a function of field was measured at room temperature on a LakeShore 7407 vibrational magnetometer. A sample with a surface area of about 1.5 cm^2 was flattened and fixed to a flat holder. The sample frequency vibration was 82 Hz. The measurements were made at orienting sample planes perpendicular (parallel to the nanowire axis, $\varphi = 0°$) and parallel (perpendicular to the nanowire axis, $\varphi = 90°$) to the external field vector. The field strength ranged cyclically from 5 to -5 kOe.
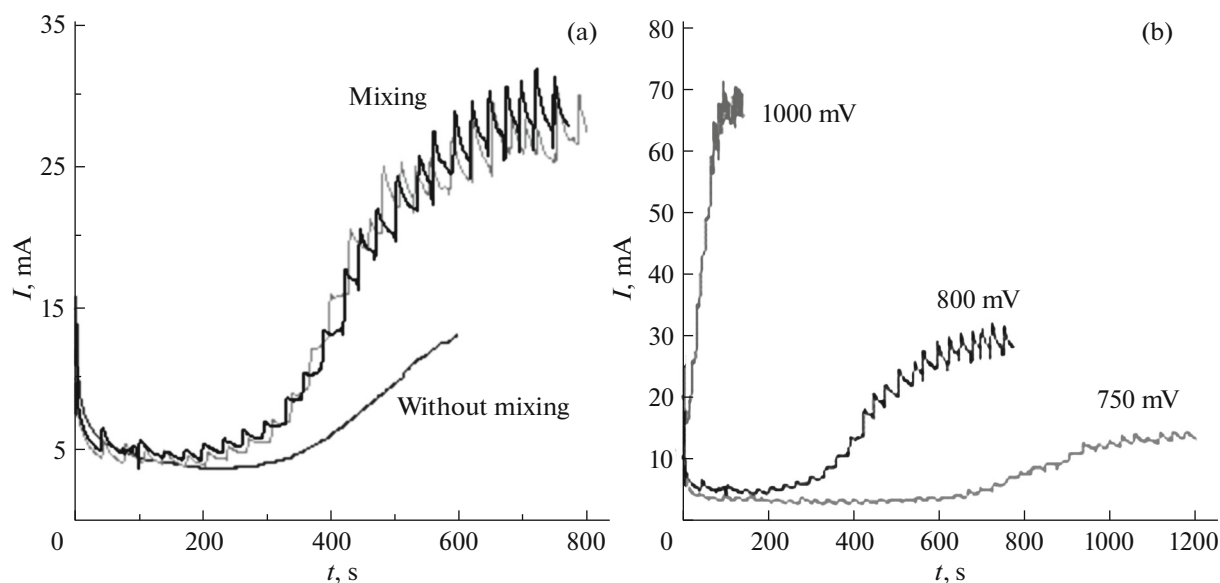
Fig. 1. Potentiograms of the growth of Fe NW arrays: (a) growth at a potential of 800 mV, the stirring effect (bottom—no stirring, top—stirring at different rate), (b) the influence of the growth potential (750, 800, and 1000 mV).

2.6. Mössbauer Spectroscopy of Samples

The Mössbauer absorption spectra on Fe-57 nuclei were recorded at room temperature on a MS-1104Em spectrometer in the constant acceleration modes with a source of $^{57}Co(Rh)$ gamma-quanta.

The isomeric shears are given relatively the standard α-Fe absorber (a 18 μm-thick foil of natural iron annealed in hydrogen). A precollimated gamma-radiation stream was directed perpendicular to the plane of the polymer matrix, and the direction of the k_γ vector matched that of the axis of tracks and nanowires. The experimental spectra were processed in the Univem MS software making part of a MS-1104Em spectrometer as well as in SpectrRelax [28] and DISCVER [29, 30] programming tools.

3. RESULTS

3.1. Electric Deposition

Iron NWs. The potentionstatic curves acquired during the synthesis of iron NW array are plotted in Fig. 1 (by example of a deposition in matrices with pore diameters of 200 nm). The influence of stirring and changed potential is evident.

The curves show the nonlinear dependence of current on time, which corresponds to the nonlinear rate of filling of pores. The significantly accelerated growth in stirring is highlighted as well. This seems to be due to increasing diffusion and to the removal of gas bubbles blocking the outputs of pore channels (note that the active release of hydrogen is the feature of galvanic deposition of iron). There is also a strong dependence of rate on voltage.

The results were used at the follow-up stage of growth from binary composition electrolytes. The currents versus the deposition times for Fe−Co and Fe−Ni are plotted in Figs. 2 and 3, respectively.

These data will definitely allow the evaluation of NW growth rate, which is high under the defined conditions. So, for Fe−Co NWs (with diameter of 100 nm) at voltages of 750, 800, and 850 mV these are 2, 6, and 20 μm/min, respectively. The NW growth rate in pores with greater diameters is much lower, as is seen in Fig. 2b.

The general view of chronoamperograms of deposited binary NW and their comparison with earlier obtained curves for pure iron group metals allows the conclusion that electric deposition of Fe−Co and Fe−Ni alloys in TM pores obeys the same regularities as the growth of NWs from pure metals (e.g., [17, 18]). In particular, filling the pores of larger diameter preserves the quasi-constant growth rate of wires, whereas filling the narrower pores results in a minimum growth rate of wires, which seems to be due to diffusion restrictions that arise in pores with predominately small diameters and higher growth rates (i.e., at high voltages). Notice that the diffusion restriction at electrodeposition in pores was reported in [31].

The effect of applying some alloying elements is also demonstrated in the conducted experiments. The positive influence of ascorbic acid ($C_6H_8O_6$; 1−2 g/L) and sodium lauryl sulfate ($NaC_{12}H_{25}SO_4$; 1 g/L) was shown as well. Ascorbic acid is known to inhibit the oxidation of bivalent iron ions with oxygen and to impair the accumulation of trivalent iron ions in electrolyte as well as their hydrolysis products that deteriorate the quality of the sediment and reduce the cur-
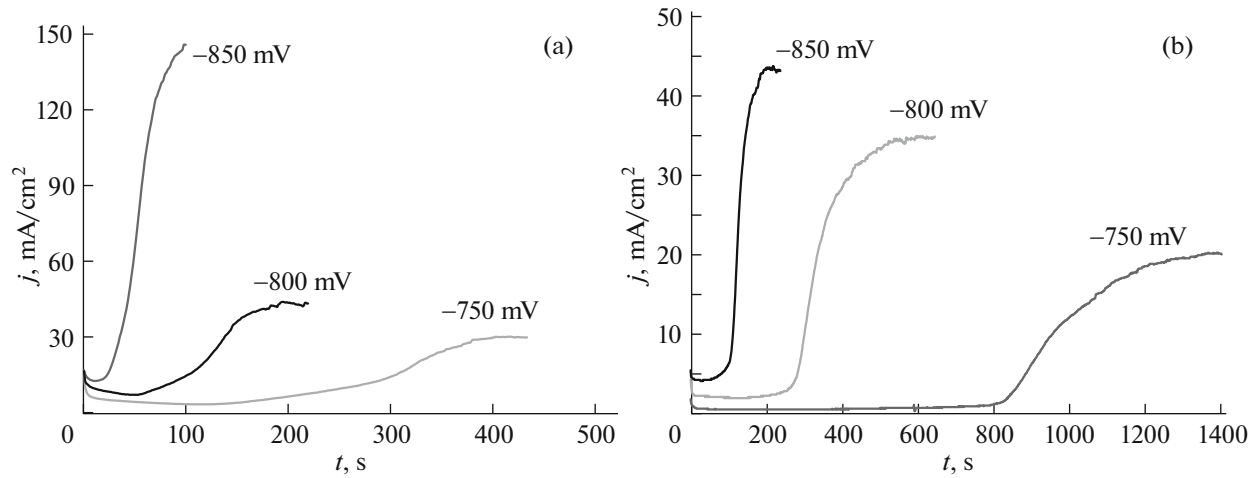
Fig. 2. Potentiograms of the deposition of Fe−Co alloy NW array at various growth voltages: (a) NW with a diameter of 100 nm, (b) NW with a diameter of 200 nm.
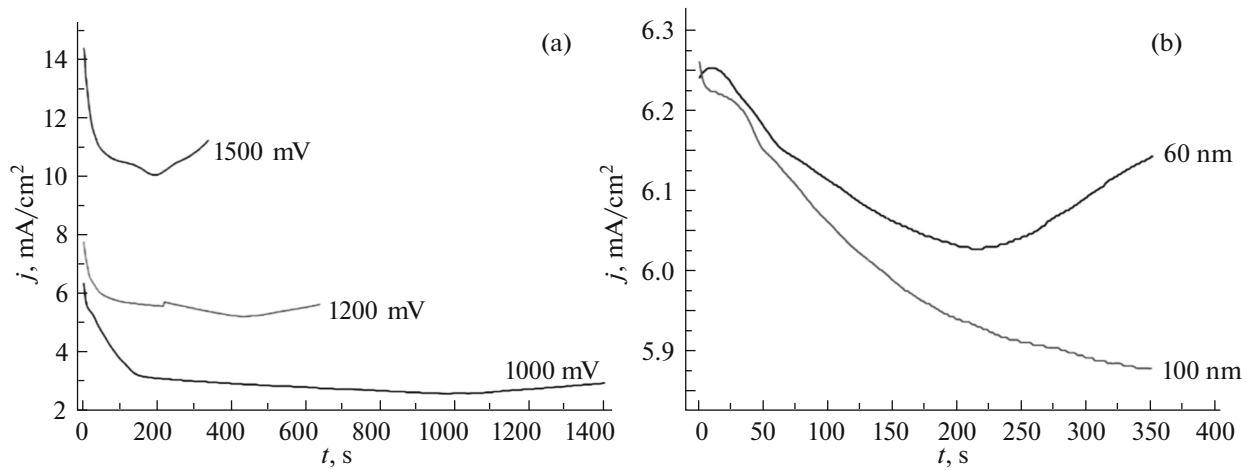
Fig. 3. Potentiograms of the deposition of Fe−Ni NW array: (a) NW with a diameter of 100 nm, (b) NW with diameters of 60 and 80 nm (denoted in plots).

rent yield of the alloy. In this case, using this acid stabilizes the composition of the electrolyte and increases its stability during the electric deposition. Lauryl sulfate served as a wetting additive, allowing one to get rid of pitting (hydrogen that releases on the anode). The acid was used for increasing the electric conductivity of electrolyte.

The produced material was composed of metal wires—filaments—piercing the thickness of a polymer matrix and being a so-called metal polymer composite. For most experiments, this composite was studied. Nevertheless, in some cases, i.e., in microscopic studies conducted below, the metal had to be separated from the polymer matrix. For this, the latter was diluted in a concentrated alkali solution. In some experiments, the process was implemented under the softer conditions, subjecting a composite to preirradi-

ation with ultraviolet ($\lambda = 310$ nm, the exposure time is 24 h). Such a treatment caused partial destruction of the polymer, making simpler its dissolution. After the separation from the matrix, there was a NW array on the common copper base.

3.2. Microscopy

The obtained SEM images of NW arrays of iron and iron−cobalt alloy are shown in Fig. 4. The NW arrays of iron−nickel alloy were examined via the scanning electron and transmission electron microscopies (see Fig. 5).

The microanalysis data of the individual NW allow the assumption that two metals are uniformly distributed within the bulk of the wire. (As seen, oxygen is concentrated on the surface, which seems to be due to the oxidation of the NW surface.) The microanalysis
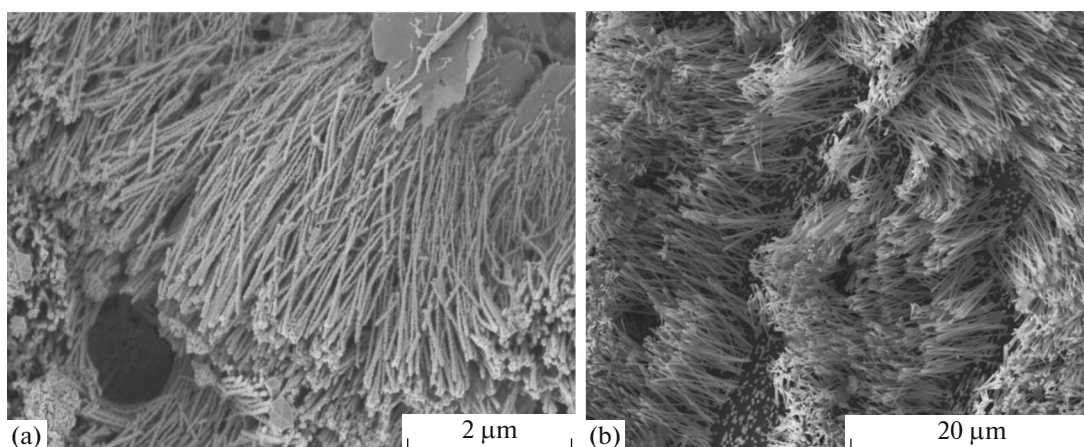
Fig. 4. SEM images: (a) Fe NW array (a 100-nm diameter and a growth voltage of 1000 mV), (b) Fe−Co NW array with 200-nm diameter, the growth voltage is 750 mV; the composition (according to microanalysis data) is: iron 82%, cobalt 18%.
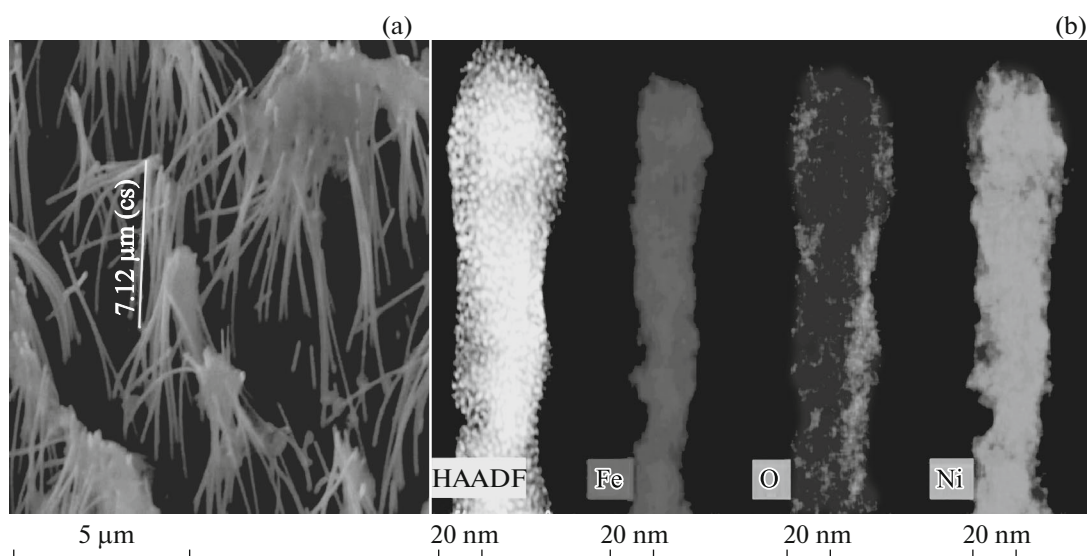
Fig. 5. Images of Fe−Ni NW arrays: (a) SEM image; (b) TEM image and corresponding distribution maps of iron, nickel, and oxygen.

was made via SEM at various sites of the array. The data (for the NW array synthesized from the electrolyte with high (50%) iron content) are presented in Fig. 6. The appropriate element analysis results for three selected areas are listed in Table 1.

Table 1. Element analysis of selected areas in a Fe−Ni NW sample

Element	Fe, at %	Ni, at %
Area 1	57.37	42.63
Area 2	53.31	46.69
Area 3	51.73	48.27

Notice that Table 1 is normalized with respect to the ratios over two elements. The full elements analysis reveals the presence of copper in the NW areas directly adjacent to the copper substrate. A small amount of cobalt is also detected in the anode.

The element analysis of NWs grown from the electrolyte with the low iron content was conducted at different growth voltage. The results are given in Table 2.

The data analysis allows the conclusion that the element ratio in two-component NWs is always different from that in the growth solution and strongly varies with the growth conditions. The iron concentration in all cases is higher than in the electrolyte (although the Fe precipitation potential is higher). This can be due to the so-called effect of "abnormal electrodeposition,"
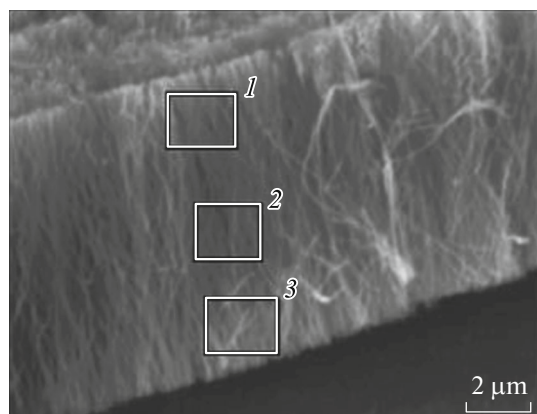
Fig. 6. SEM image of Fe−Ni NW arrays (the NW diameter is 60 nm, and the growth voltage is 1500 mV). The areas exposed to the element analysis are shown with rectangles. (The copper substrate—the growth base—is at the bottom.)

Fig. 7. X-ray diffractograms of pure iron NW arrays, acquired at different growth voltages. (Bottom—the control spectrum of copper deposited onto a flat surface; the lines of copper are also shown in spectra.)

which has earlier been observed for analogous deposition of metals on a flat surface.

The element composition is also found to noticeably alter along the NWs. The change in the iron-to-nickel (Fe/Ni) element ratio is slightly increased upon the growth. This can be interpreted by different ion mobility and electric deposition conditions at various sites of the narrow pore.

The microscopy also enables the topographic analysis of arrays, evidencing the regular geometric (cylindrical) shape of NWs and their small length distribution in the array. These positive moments are perhaps due to leveling additives in electrolytes. The measured NW diameters are found to be a little bit greater than those reported by the producer for the growth matrix. This effect is obvious for pores and NWs of small diameters, because the approach applied for evaluating the pore parameters (a so-called Hagen−Poisseuille method) is not enough accurate, often giving the understated integral value. Another reason is a slight broadening, or "extension," of the polymer of the growing NW.

3.3. X-ray Diffraction Analysis

Iron NWs. Figure 7 displays the X-ray spectrograms of pure iron samples grown at different voltages.

The spectrum corresponds to that of alpha-iron with a bcc lattice. The lattice parameter is almost independent on the growth rate, being 2.8657 Å for a growth voltage of 750 mV. This value is smaller than the corresponding parameter of 2.8665 Å for the bulk iron, which can be owing to some "lattice compression" upon the growth of a metal in the pore channel. The lines of iron lose intensity with increasing growth voltage (and respectively with higher growth rate),

presumably because of larger crystallite dimensions and/or greater lattice distortions.

Iron−cobalt NWs. The X-ray diffractograms were also recorded on iron−cobalt NW arrays obtained at growth voltages of 700, 750, 800, and 850 mV. No lines of cobalt are observed in spectrograms, meaning the formation of an iron-based solid solution with cobalt, slightly changing the lattice parameters. It is worth mentioning that the formation of solid solution for macroscopic samples is expected and is fully consistent with the phase diagram. The lines attributed to the alloy have a large width of $0.65° \pm 0.1°$, due to small coherent domain sizes and/or great distortions. In all cases, the lines of the alloy and the lattice parameters, calculated from them, are close to those of iron. So, the average lattice parameter is 2.855 Å, being below the reference value of 2.8664 Å for pure bcc iron [32].

The X-ray spectrogram of iron−cobalt NW samples produced at the same growth voltage in the matrices with pores of different diameters is shown in Fig. 8.

According to the analysis of curves, the NW is a solid solution of cobalt in bcc iron. In this case, the lattice parameters of samples obtained under various conditions are slightly different, ranging from 2.854 to 2.866 Å. It is noticeable that the intensity of the (111, bcc) peak decreases with enlarging pore diameter, which can be due to the influence of boundaries (pore walls), surface, and magnetic interaction between particles.

Table 2. Element analysis of Fe−Ni NW samples synthesized at different voltages

| Element	1000 mV	1200 mV	1500 mV
Fe	17.66%	7.57%	6.49%
Ni	82.34%	92.43%	93.51%
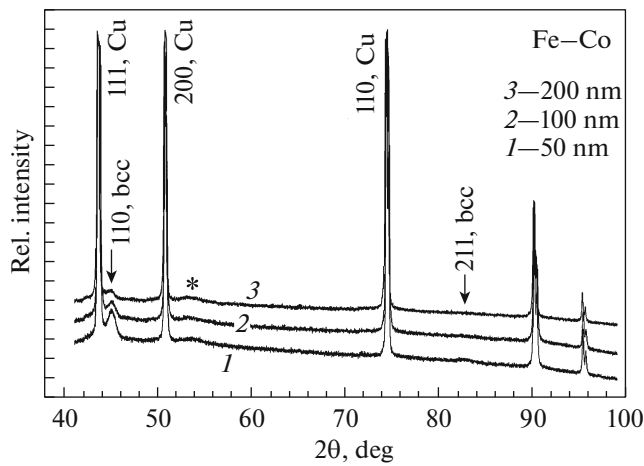
Fig. 8. X-ray spectrograms of Fe−Co NW arrays obtained in matrices with pores of diameters of 50, 100, and 200 nm. (The growth voltage is 750 mV.) The lines of copper are denoted as well. The star is attributed to the peaks of a polymer matrix.
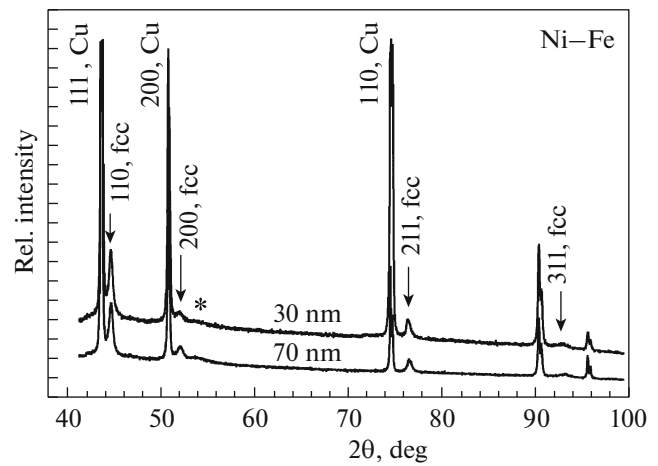
Fig. 9. X-ray spectrograms of Ni−Fe (6.5% Fe) NW arrays obtained in matrices with pores of diameters of 30 and 70 nm. (The growth voltage is 1500 mV.) The lines of copper are denoted as well. The star is attributed to the peaks of a polymer matrix.
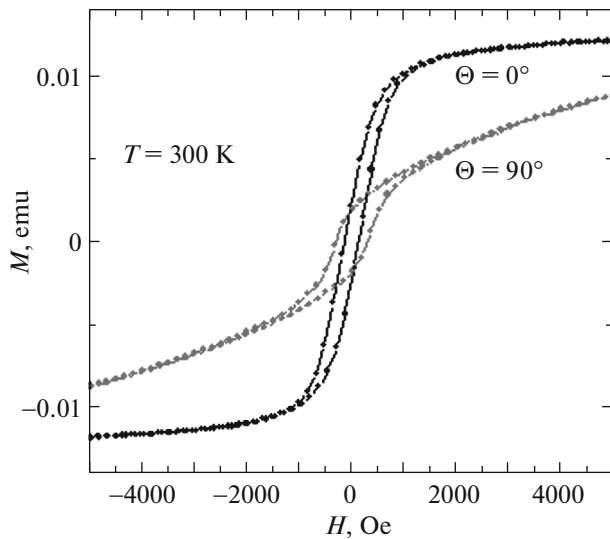
Fig. 10. Hysteresis loop for NW array (100-nm pores).
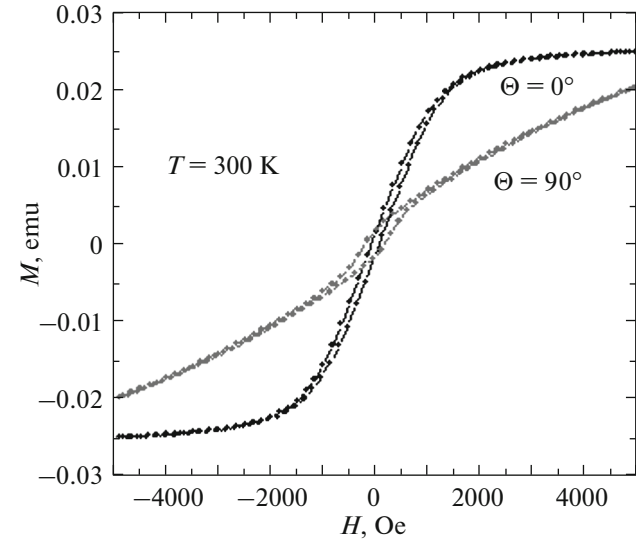
Fig. 11. Hysteresis loop for NW array (200-nm pores).

The X-rays difractogram of the iron−nickel NW array in a matrix with two different pore diameters is shown in Fig. 9.

The X-ray data analysis reveals that the NW is a γ−Ni−Fe solid solution with an fcc lattice structure typical of the nickel-rich bulk phases.

3.4. Magnetometry

The magnetic properties of pure-iron NWs. The magnetic characteristics of nanowires of pure iron were studied as well, at obtaining the orientation dependences for two samples of pure iron with pores of 100 and 200 nm. The measurements were made for the parallel and perpendicular orientations of the external magnetic field relative to the normal to the film surface ($\theta = 0°$ and $\theta = 90°$, respectively). The acquired magnetization curves are plotted in Figs. 10 and 11.

It is clear that, for iron NWs obtained in pores with smaller diameters, the magnetic hysteresis loops are broader because of strong spatial anisotropy of NW, and, consequently, the dedicated orientation of magnetic moments of domains along the NWs in wires with smaller diameters.

This situation is typical of magnetization curves for all the studied compositions of NWs. An unusual ratio of shapes (widths) of hysteresis loops for two orienta-
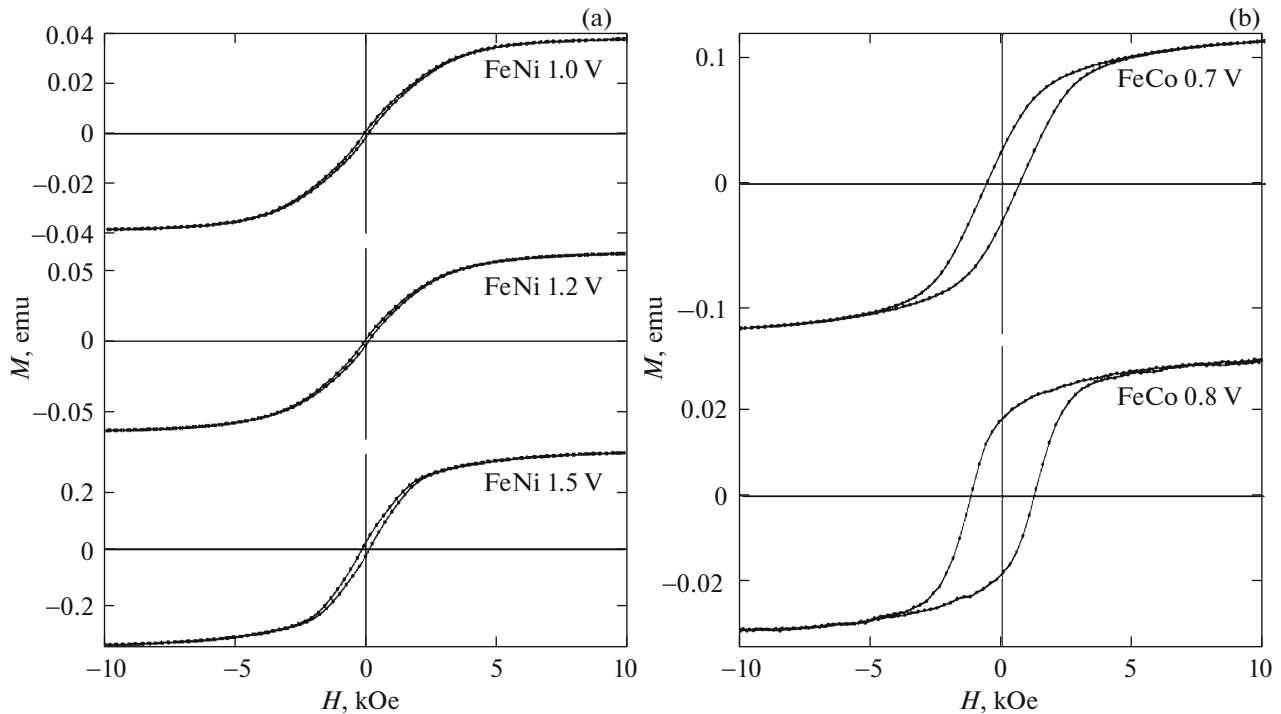
Fig. 12. Hysteresis loops for: (a) iron−cobalt samples; (b) for FeCo samples.

tions of the external magnetic field attracts attention. In a common case of domains with axial magnetic anisotropy, the hysteresis loop width is expected to be maximal when the field is oriented along a "light," i.e., NW, axis, while the magnetization curve is almost paramagnetic (loop-free) for perpendicular orientation. It is worth mentioning that the loop is quite narrow for a sample with a NW diameter of 200 nm, where the magnetic properties are close to those of the conventional magnetosoft material.

The measured data for nonoriented iron−cobalt and iron−nickel samples are shown in Fig. 12.

For FeCo samples, the coercive force and remaint magnetization are calculated to be respectively 630 and 1100 Oe and 27 and 18 memu; i.e., these samples are magnetohard. Unlike iron−cobalt systems, the coercive force and remain polarization for FeNi samples are found to be 75, 80, and 140 Oe and 1, 1.3, and 2.2 memu; i.e., the latter are attributed to magnetosoft materials.

As observed for both series of samples, the higher is the growth voltage, the greater are the magnetohard characteristics; i.e., there is a rise in coercive force and remaint magnetization. This can be assumed to be due to the fact that increasing the growth rate leads to the formation of fine-grained structure (as is indirectly evidenced by XRD data).

The hysteresis loops for iron−nickel samples (with NWs of different diameters and orientations) are plotted in Fig. 13. One observes a typical orientation dependence, i.e., for a field co-directed with the NW axis (zero inclination), a hysteresis loop is much broader than for a field making a 90° angle with a NW axis. Notice that the nickel alloy for NWs with small diameters behaves itself as the magnetohard materials.

3.5. Mössbauer Spectroscopy

The Mössbauer spectra for all NW array samples evidence the characteristic magnetic splitting and are composed of weakly broadened sextets (Figs. 14−16). The greater broadening of spectra of Co−Fe and Ni−Fe NWs seems to be a result of the distribution of hyperfine interaction parameters because of the forming several positions of iron ions in the bcc lattice of a cobalt or nickel matrix [16].

The spectra of pure iron NW arrays obtained at various deposition potentials have similar hyperfine parameters to the bulk materials. However, at potentials above the absolute value of 800 mV, the Mössbauer spectra reveal the presence of low-intensity paramagnetic doublets from the appropriate iron ions in Fe−Cu alloys, which form at the onset of deposition on a copper substrate [20]. Besides this, the intensities I_i of lines i of a Mössbauer sextet ($I_{1.6} : I_{2.5} : I_{3.4}$) in a sample obtained at a potential of −750 mV are found to be different from a value of 3 : 2 : 1, which is characteristic of the randomly oriented magnetic moments in polycrystalline bulk samples.
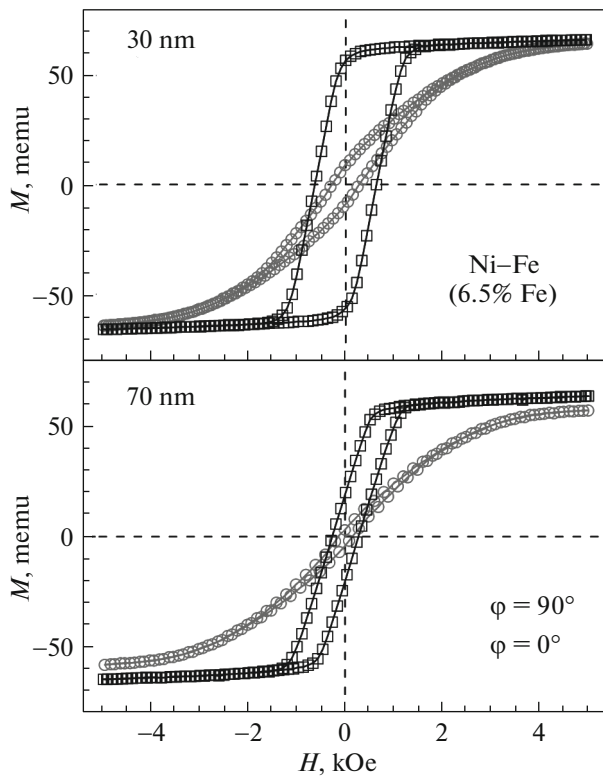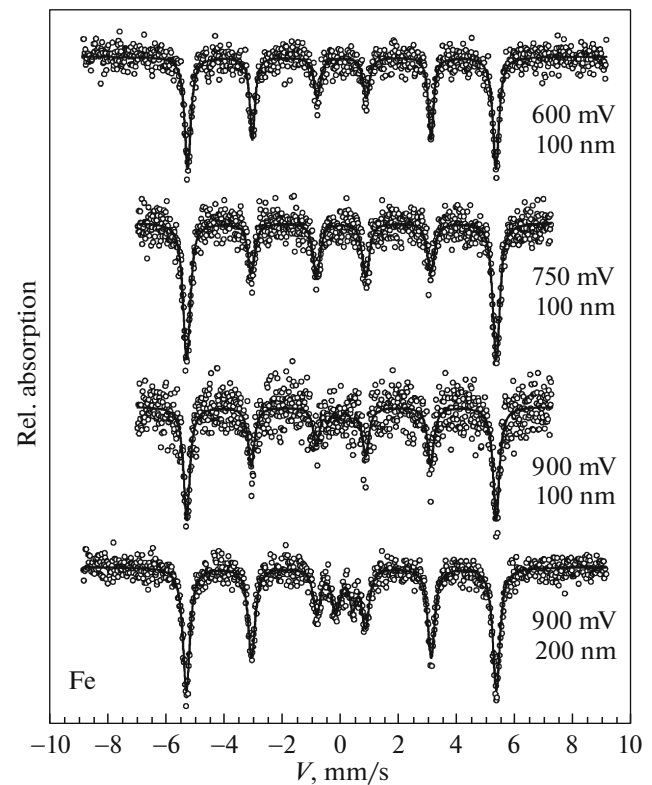
Fig. 13. Hysteresis loops of Ni−Fe samples with different NW diameters at various orientations of the external field.


Fig. 14. Mössbauer spectra of Fe samples grown in pores with 100-nm diameters at different potentials: 600, 750, 900 mV, and in pores with 200-nm diameters (at a potential of 900 mV).

In the magnetic hyperfine structure of the Mössbauer spectrum, the I_i values obey the ratios of $I_{1.6} : I_{3.4} = 3$ and $I_{2.5} : I_{3.4} = A_{2.5} = 4\sin^2\theta_k/(1 + \cos^2\theta_k)$, where θ_k is the angle between the wave vector of the gamma quantum $\mathbf{k}_\gamma$ and the direction of the magnetic field B_{hf} [33]. For the perfect orientation of "light" axes and magnetic moments parallel to the $\mathbf{k}_\gamma$ vector, $\theta_k = 0$ and $A_{2.5} = 0$. As shown in [34], the magnetic moments of single-domain spherical particles with diameters less than 20 nm in chains will be antiferromagnetically ordered along the chains. The lines *2* and *5* must therefore completely vanish in the magnetic sextet of nanowires with diameters below 20 nm [35]. The different orientations of "light" axes and/or the violation of the single-domain cross-section in NWs with increasing their diameters causes the averaging of the Mössbauer spectra over the hyperfine parameter distribution, which is determined by the mean value of $\left\langle \cos^2\theta_k \right\rangle$ [36]. In turn, the mean values of θ_k angles found by the formal analysis of the $A_{2.5}$ parameter are as follows:

$$\left\langle \cos^2\theta_k \right\rangle = (4 - A_{2.5})/(4 + A_{2.3}). \qquad (1)$$

For better clarity, the directions of the "light" axes in the NW array and the orientations of the magnetic moments can be assumed to be uniformly distributed around the direction of $\theta_k = 0$ in a range of $\Delta\Theta$ ($0 < \Delta\Theta < \pi/2$) over the polar angle; i.e., in a cone of directions with a solution $2\Delta\Theta$ relative to the nanowire axis. Then

$$\left\langle \cos^2\theta_k \right\rangle_{\Delta\Theta} = \frac{1 - \cos^3\Delta\Theta}{3(1 - \cos\Delta\Theta)}, \qquad (2)$$

and a certain value $\Delta\Theta$ for each spectrum will be defined by the $A_{2.5}$ ratio by combining the expressions (1) and (2).

For NW arrays of binary compounds, the violation of intensity ratios is observed in Mössbauer spectra of the all studied samples (see Figs. 15 and 16). The orientation of magnetic moments in a wire is found to depend mainly on the diameter of track pores d, and to a lesser extent on the deposition potential (i.e., on the NW growth rate). For NWs obtained in pores with diameters below 100 nm, the magnetic moments are predominantly directed at angles of 0–40° relative to the NW axis, and the maximum angle Θ of the deviation from the axis ranges from 30° to 40°. For NWs produced in pores with diameters of 200 nm, the $I_{1.6} : I_{2.5} : I_{3.4}$ intensity ratio of lines in a sextet becomes close to 3 : 2 : 1 for the bulk polycrystalline sample (Fig. 14).
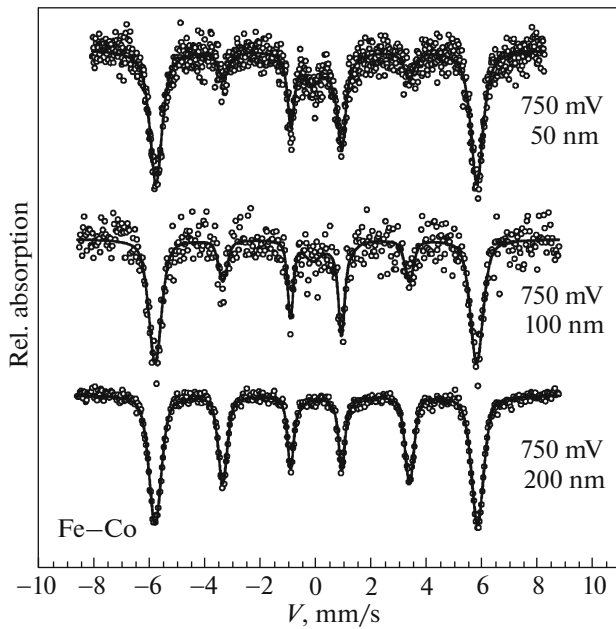
Fig. 15. Mössbauer spectra of Fe−Co NW arrays with NW diameters of 50, 100, and 200 nm (the growth voltage was 750 mV).
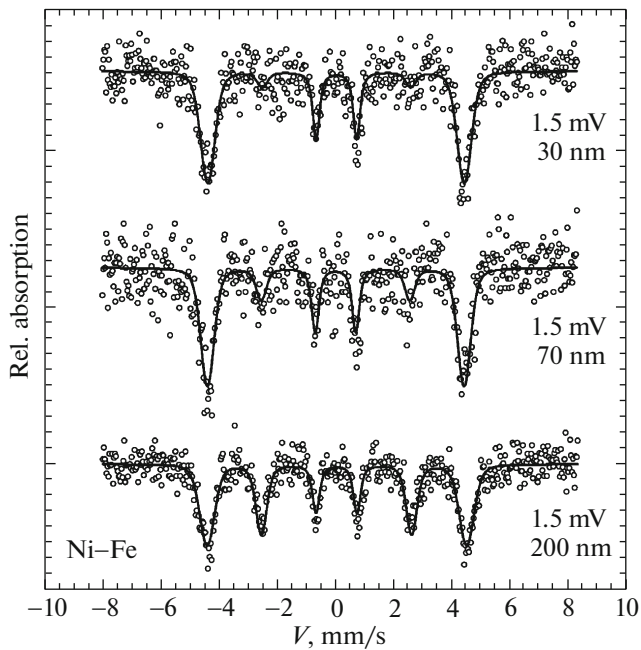
Fig. 16. Mössbauer spectra of Fe−Ni NW arrays.

The spectra of iron−cobalt NW arrays (with different diameters) are shown in Fig. 15.

It is obvious that only the NWs with diameters of 200 nm give a sextet with the classical intensity ratio of 3 : 2 : 1, typical of bulk nonoriented alpha-iron. The change in the arbitrary intensities of the second and fifth lines in spectra of NWs with smaller diameters

evidences the presence of the preferred direction of magnetization.

The Mössbauer spectra of Fe−Ni NWs are shown in Fig. 16.

As follows from the Mössbauer spectroscopy data, the FeCo alloy may be composed of three phases, while FeNi exhibits two phases. The metal deposition in pores with greater diameters as well as the deposition at low rates results in NWs whose properties are close to the bulk materials. It is worth mentioning that, unlike the earlier studied pure iron NWs where spontaneous magnetization arises at certain conditions, all the alloy samples in the present work exhibit magnetization. The field at ^{57}Fe cores in FeCo NWs is about 3 T greater than for pure iron NWs, whereas that for FeNi alloy is 5 T less than for pure iron NWs.

4. CONCLUSIONS

The growth matrix parameters and growth conditions were found to exert influence on all the characteristics of NW arrays. Varying the growth makes greater contribution than the change in pore channel diameters. As established for all samples, the lower was the growth rate (i.e., at the minimum growth voltage), the closer were the properties of NWs to the bulk materials, as was also observed with increasing the pore diameters. NWs with diameters of 200 nm exhibited predominately the properties of the bulk material. The element composition of the binary NW arrays (alloys) was different from that of electrolyte, first of all, by the relatively increased iron concentration, depending on the synthesis conditions. Furthermore, the NW composition varied with length.

The fundamental ability to tune the magnetic properties of nanowires upon their synthesis by varying the composition of the electrolyte, the deposition rate and the pore diameter was thereby shown. However, the production of nanowires with predetermined magnetic properties still necessitates a large amount of complementary experiments, i.e., with involving the external magnetic fields.

REFERENCES

1. V. M. Anishchik, *Nanomaterials and Nanotechnology*, Ed. by V. Borisenko and N. Tolochko (Belorus. Gos. Univ., Minsk, 2008) [in Russian].

2. G. E. Possin, Rev. Sci. Instrum. **41**, 772 (1970).

3. S. Kawai and R. J. Ueda, Electrochem. Soc. **112**, 32 (1975).

4. S. K. Chakarvarti and J. Vetter, Nucl. Instrum. Methods Phys. Res. **62**, 109 (1991).

5. J. Vetter and R. Spohr, Nuclear Instrum. Methods Phys. Res. **79**, 69 (1993).

6. T. M. Whitney, J. S. Jiang, P. C. Searson, and C. L. Chien, Science (Washington, DC, U. S.) **261**, 1316 (1993).

7. C. R. Martin, Science (Washington, DC, U. S.) **266**, 1961 (1994).

8. N. Lupu, *Electrodeposited Nanowires and Their Applications*, Ed. by N. Lupu (InTech, Croatia, 2010).

9. *Magnetic Nano- and Microwires: Design, Synthesis, Properties and Applications*, Ed. by M. Va'zquez (Woodhead, Elsevier, 2015).

10. A. A. Davydov and V. M. Volgin, Russ. J. Electrochem. **52**, 806 (2016).

11. H. Masuda and K. Fukuda, Science (Washington, DC, U. S.) **268**, 1466 (1995).

12. A. Schulz, G. N. Akapiev, V. V. Shirkova, H. Rosler, and S. N. Dmitriev, Nucl. Instrum. Methods Phys. Res., Sect. B **236**, 254 (2005).

13. A. Dangwal, C. S. Pandey, G. Muller, S. Karim, T. W. Cornelius, and C. Trautmann, Appl. Phys. **92**, 063115 (2008).

14. D. L. Zagorski, S. A. Bedin, V. A. Oleinikov, N. B. Polyakov, O. G. Rybalko, and B. V. Mchedlishvili, Rad. Meas. **44**, 1123 (2009).

15. D. Dobrev, J. Vetter, N. Angert, and R. Neumann, Appl. Phys. A **72**, 729 (2001).

16. K. V. Frolov, D. L. Zagorskii, I. S. Lyubutin, V. V. Korotkov, S. A. Bedin, S. N. Sulyanov, V. V. Artemov, and B. V. Mchedlishvili, JETP Lett. **99**, 570 (2014).

17. V. V. Korotkov, V. H. Kudryavtsev, D. L. Zagorskii, and S. A. Bedin, Gal'vanotekh. Obrab. Poverkhn. **19** (4), 23 (2011).

18. V. V. Korotkov, V. N. Kudryavtsev, S. S. Kruglikov, D. L. Zagorskii, S. N. Sul'yanov, and S. A. Bedin, Gal'vanotekh. Obrab. Poverkhn. **23** (1), 24 (2015).

19. I. Shao, M. W. Chen, R. C. Cammarata, P. C. Searson, and S. M. Prokesc, J. Electrochem. Soc. **154**, 572 (2007).

20. K. V. Frolov, D. L. Zagorskii, I. S. Lyubutin, M. A. Chuev, I. V. Perunov, S. A. Bedin, A. A. Lomov, V. V. Artemov, and S. N. Sulyanov, JETP Lett. **105**, 319 (2017).

21. D. C. Leitao, C. T. Sousa, J. Ventura, J. S. Amaral, F. Carpinteiro, K. R. Pirota, M. Vazquez, J. B. Sousa, and J. P. Araujo, J. Non-Cryst. Solids **354**, 5241 (2008).

22. M. Almasi Kashi, A. Ramazani, S. Doudafkan, and A. S. Esmaeily, Appl. Phys. A **102**, 761 (2011).

23. W. Pangpang, G. Lumei, W. Liqun, Z. Dongyan, Y. Sen, and S. Xiaoping, Int. J. Phys. B **24**, 2302 (2010).

24. Q. Zhan, Z. Chen, D. Xue, F. Li, H. Kunkel, X. Zhou, R. Roshko, and G. Williams, Phys. Rev. B **66**, 134436 (2002).

25. Z. Chen, Q. Zhan, D. Xue, F. Li, X. Zhou, H. Kunkel, and G. Williams, J. Phys.: Condens. Matter **14**, 613 (2002).

26. Q. Zhan, J. Gao, Y. Liang, N. Di, and Z. Cheng, Phys. Rev. B **72**, 024428 (2005).

27. M. Schlesinger and M. Paunovic, *Modern Electroplating* (Wiley, New York, 2010).

28. M. E. Matsnev and V. S. Rusakov, AIP Conf. Proc. **1489**, 178 (2012).

29. A. M. Afanas'ev and M. A. Chuev, J. Exp. Theor. Phys. **80**, 560 (1995).

30. M. A. Chuev, Dokl. Phys. **56**, 318 (2011).

31. L. Movsesyan, I. Schubert, L. Yeranyan, C. Trautmann, and M. E. Toimil-Molares, Semicond. Sci. Technol. **31**, 1 (2016).

32. A. A. Rusakov, *X-Ray Diffraction of Metals* (Atomizdat, Moscow, 1977) [in Russian].

33. V. S. Shpinel', *Resonance of Gamma-Rays in Crystals* (Nauka, Moscow, 1969) [in Russian].

34. I. S. Jacobs and C. P. Bean, Phys. Rev. **100**, 1060 (1955).

35. Z. Chen, Q. Zhan, D. Xue, F. Li, X. Zhou, H. Kunkel, and G. Williams, J. Phys.: Condens. Matter **14**, 613 (2002).

36. M. A. Chuev, V. M. Cherepanov, and M. A. Polikarpov, JETP Lett. **92**, 21 (2010).

Translated by O. Maslova